Available online at www.sciencedirect.com
ScienceDirect
Journal of Volcanology and Geothermal Research 161 (2007) 261–274
Journal of volcanology and geothermal research
www.elsevier.com/locate/jvolgeores

Petrologic constraints on the decompression history of magma prior to Vulcanian explosions at the Soufrière Hills volcano, Montserrat

A.B. Clarke [a,*], S. Stephens [b], R. Teasdale [c], R.S.J. Sparks [b], K. Diller [a]

[a] School of Earth and Space Exploration, Arizona State University, Tempe, AZ 85287-1404 USA
[b] Department of Earth Sciences, Bristol University, Bristol, England UK
[c] Department of Geological and Environmental Sciences, California State University at Chico, Chico, CA USA

Received 1 September 2005; received in revised form 22 November 2006; accepted 27 November 2006
Available online 16 January 2007

Abstract

A series of 88 Vulcanian explosions occurred at the Soufrière Hills volcano, Montserrat, between August and October, 1997. Conduit conditions conducive to creating these and other Vulcanian explosions were explored via analysis of eruptive products and one-dimensional numerical modeling of magma ascent through a cylindrical conduit. The number densities and textures of plagioclase microlites were documented for twenty-three samples from the events. The natural samples all show very high number densities of microlites, and >50% by number of microlites have areas <20 μm^2. Pre-explosion conduit conditions and decompression history have been inferred from these data by comparison with experimental decompressions of similar groundmass compositions. Our comparisons suggest quench pressures <30 MPa (origin depths <2 km) and multiple rapid decompressions of >13.75 MPa each during ascent from chamber to surface. Values are consistent with field studies of the same events and statistical analysis of explosion time-series data. The microlite volume number density trend with depth reveals an apparent transition from growth-dominated crystallization to nucleation-dominated crystallization at pressures of ~7 MPa and lower. A concurrent sharp increase in bulk density marks the onset of significant open-system degassing, apparently due to a large increase in system permeability above ~70% vesicularity. This open-system degassing results in a dense plug which eventually seals the conduit and forms conditions favorable to Vulcanian explosions. The corresponding inferred depth of overpressure at 250–700 m, near the base of the dense plug, is consistent with depth to center of pressure estimated from deformation measurements. Here we also illustrate that one-dimensional models representing ascent of a degassing, crystal-rich magma are broadly consistent with conduit profiles constructed via our petrologic analysis. The comparison between models and petrologic data suggests that the dense conduit plug forms as a result of high overpressure and open-system degassing through conduit walls.

Keywords: quench pressure; conduit dynamics; Vulcanian; explosive eruptions; conduit modelling; conduit dynamics

1. Introduction

The current eruption of the Soufrière Hills volcano (SHV) is characterized primarily by effusive dome building with intermittent periods of explosive activity (Young et al., 1998). Between August and October 1997, 88 pyroclastic-flow-producing Vulcanian explosions occurred with a mean repose of just 9.5 h and mean high-flux-phase duration of tens of seconds (Druitt et al., 2002). Up to 10^6 m^3 of andesite magma (dense rock equivalent, DRE) were ejected at speeds up to 170 m s^{-1},

* Corresponding author. Tel.: +1 480 965 6590; fax: +1 480 965 8102.
E-mail address: amanda.clarke@asu.edu (A.B. Clarke).

0377-0273/$ - see front matter
doi:10.1016/j.jvolgeores.2006.11.007

and plumes reached as high as 15 km above sea level (Druitt et al., 2002). The average inter-explosion magma flux rate was 3–13 m^3 s^{-1} (based on erupted volumes and time between eruptions, Druitt et al., 2002). A statistical study of the time series of explosions in September and October 1997 indicates that each batch of magma experienced 6 to 8 episodic decompressions between leaving the chamber and erupting at the surface, recording 60–87 h of eruptive history (Jaquet et al., 2006).

Several studies have suggested that the transition from effusive to explosive eruptive behavior and variations in explosion scale can be explained by changes in conduit dynamics (Jaupart and Allegre, 1991; Woods and Koyaguchi, 1994; Melnik and Sparks, 2002, 2005), including changes caused by exsolution of volatiles, degassing of the system via permeability (Taylor et al., 1983; Eichelberger et al., 1986; Jaupart, 1998), groundmass crystallization and corresponding changes in magma rheology (Sparks, 1997; Melnik and Sparks, 1999; Massol and Jaupart, 1999; Cashman and McConnell, 2005; Mastin, 2005). Numerical models have investigated relationships between complex conduit processes and eruptive behavior (Melnik and Sparks, 1999; Papale, 1999; Barmin et al., 2002; Melnik and Sparks, 2005; Mastin, 2005). However, boundary and initial conditions, along with many simplifying assumptions, must be applied in order to solve equations for conduit flow, making empirical constraints and validation imperative. Unfortunately, subsurface data are difficult to obtain directly and parameters need to be inferred indirectly (Voight et al., 1998, 1999). Eruptive products are potential sources of data which can constrain subsurface processes.

The groundmass of pyroclastic material commonly contains tiny crystals, less than 100 μm^2 in cross-sectional area (microlites) that develop during magma ascent from chamber to quench due to degassing (e.g., Cashman, 1992; Hammer et al., 1999). Crystal textures reflect pre-explosion conduit conditions, decompression rate and style, as well as time between decompression and quench (residence time, T_r), allowing estimation of magma storage and ascent conditions (e.g., Swanson et al., 1989; Cashman, 1992; Geschwind and Rutherford, 1995; Cashman and Blundy, 2000; Hammer et al., 2000; Hammer and Rutherford, 2002; Couch et al., 2003a,b; Cashman and McConnell, 2005). Plagioclase and potassium feldspar are the dominant microlite minerals because the feldspar liquidus is strongly affected by decreasing water content in the melt (Burnham, 1979; Sisson and Grove, 1993; Moore and Carmichael, 1998; Cashman and Blundy, 2000). Plagioclase feldspar is abundant in the SHV andesite (Murphy et al., 1998; Devine et al., 1998).

Two recent experimental studies quantify relationships between groundmass crystal textures and dynamic conduit parameters, where groundmass compositions representative of both the Pinatubo (Hammer and Rutherford, 2002) and SHV systems have been explored (Couch et al., 2003a,b). Two styles of decompression were simulated; the first is decompression to final pressure (P_f) in a single step (SDEs); the second is decompression by several staggered steps of equal decompression magnitude, ΔP (MDEs). These experimental data provide a valuable framework relating feldspar crystal morphology, aspect ratio, crystal size distribution, and volume fraction to decompression (ascent) rate and style (MDE vs. SDE), quench pressure and residence time, within which natural samples can be interpreted.

This study has four parts. First, we characterize explosion samples from the 1997 SHV events by measuring clast density and groundmass plagioclase microlite morphology, volume fraction and size distribution. Second, we compare these data to experimental results (Hammer and Rutherford, 2002; Couch et al., 2003a,b) in order to constrain decompression style and quench pressure. Third, we compare our results to estimates made by field observations of the Vulcanian explosions (Druitt et al., 2002) and by a statistical study of time-series data of the same events (Jaquet et al., 2006). Fourth, we compare findings against independent calculations of a one-dimensional numerical model of magma ascent.

2. Methods

2.1. Sampling

Pumice samples from pyroclastic flow deposits formed in the 1997 Vulcanian explosions of the SHV were collected in Spring, 1999, during a period of relatively low volcanic activity. Bulk samples were collected along a traverse away from the vent within a given stratigraphic horizon and sieved to 36 mm diameter. Larger fractions were weighed to obtain mass fractions of the largest clasts, up to tens of cm in diameter. The remaining bulk samples were quartered and further sieved in the lab. Eight clasts were selected for this study from a single pyroclastic flow deposit (Fig. 1; site 1), and therefore from a single Vulcanian explosion, 1 km north of the vent (lat. 16.72773; long. 62.1858). Six additional clasts came from site 2 (lat. 16.73957; long. 62.16232). Nine additional Vulcanian-derived clasts came from other primary deposit sample locations over a 180° sector of the volcano. All clasts ranged from phi sizes $>-3\phi$ to $>-5\phi$ chosen because they

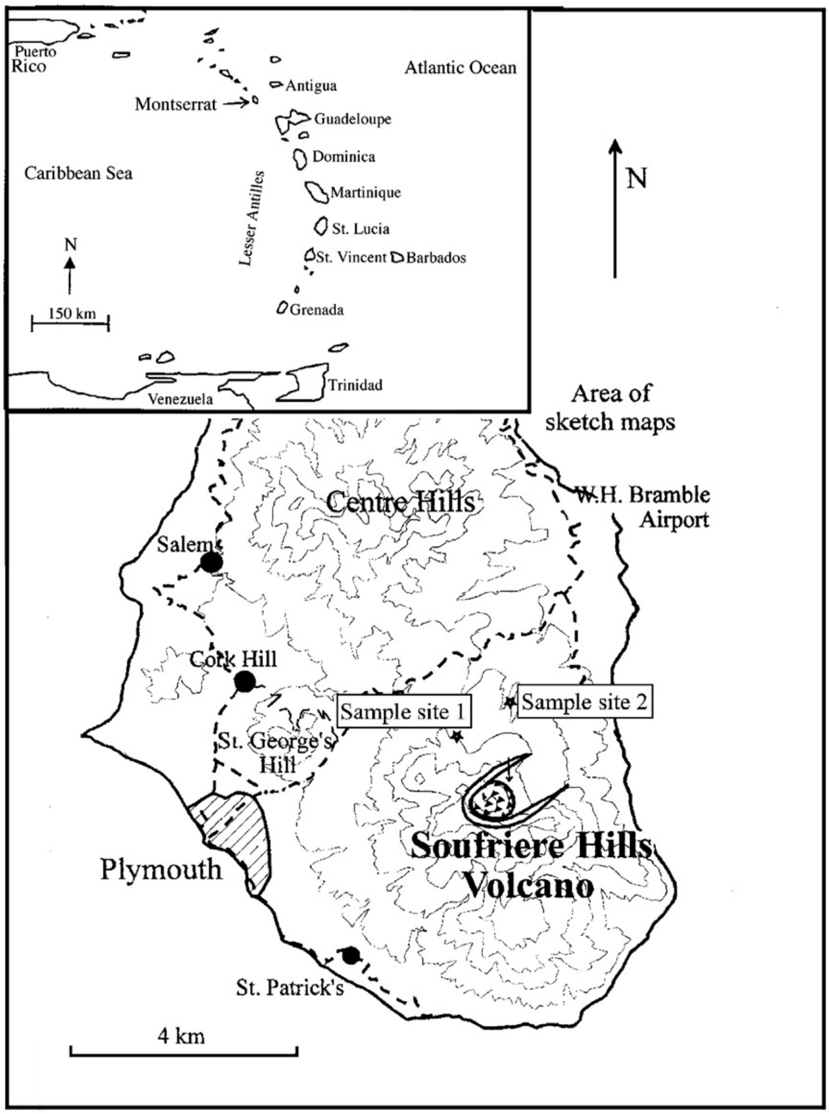

Fig. 1. Map of Montserrat, Soufrière Hills volcano and sample locations (Site 1 — lat. 16.72773, long. 62.1858; Site 2 — lat. 16.73957, long. 62.16232).

were evenly vertically distributed within the flow deposits (only coarse-tail grading was observed) and exhibited a wide range of densities. The samples, although not all from the very same explosion, are assumed to be representative of the 'average' 1997 SHV explosion.

2.2. Density measurements

The dry weight of each sample was first measured in air and then suspended in water, after sealing with plastic film and silicone water-proofing spray. Samples less dense than water were enclosed in a wire cage and suspended by a stiff stem from an electronic scale to obtain the submerged weight. Clast density was then calculated from the two measurements (Hoblitt and Harmon, 1993). Error in density measurements is +/−30 kg m^{-3} and is associated with uncertainty in mass measurements.

2.3. Textural analysis

The Hitachi S-3500N Scanning Electron Microscope in the Earth Sciences Department at the University of Bristol was used at an acceleration potential of 20 kV and working distance of 11 mm to create 1200× magnification, high gain backscatter images. Avoiding large phenocrysts, an area of groundmass (45,000–70,000 μm^2) for each sample was chosen and divided into six to nine adjacent sub-areas

Table 1

	Sample	Clast density (g cm^{-3})	Groundmass plag. (vol.%)	Microlite morphology	Vesicle area (%)	Max microlite aspect ratio	Average microlite area, s_a (μm^2)	Microlite number density, N_a (mm^{-2})	Charac. microlite size, s (μm)	Volumetric number density, N_v (mm^{-3})
Location 1	990329-1a(1)	1.471	33	Tabular hopper	48	10	45	6820	6.96	980,521
	990329-1b(1)	1.225	15	Tabular	67	11	21	12,748	3.43	3,716,328
	990329-2a(1)	0.728	32	Tabular	80	8	69	4639	8.31	558,546
	990329-3a(1)	0.989	19	Tabular	78	8	32	5876	5.69	1,033,346
	990329-3b(2)	1.263	23	Tabular	75	16	51	4015	7.57	530,548
	990329-3c(3)	0.965	29	Tabular	68	8	89	1613	13.41	120,309
	990329-4a(2)	1.218	18	Tabular	69	5	35	2196	9.05	242,509
	990329-4b(1)	0.876	28	Tabular	75	9	80	3532	8.90	396,666
	990302-5a(1)	1.194	21	Tabular	63	3	188	17,969	3.42	5,256,252
Location 2	990302-6a(1)	1.374	21	Tabular skeletal	54	19	11	18,467	3.37	5,476,131
	990302-6b(3)	0.676	11	Tabular skeletal	76	13	41	2681	6.41	418,551
	990302-7a(2)	2.352	34	Tabular	25	6	17	19,997	4.12	4,849,481
	990302-7b(4)	1.347	21	Tabular	64	9	23	8491	4.97	1,707,339
Other locations	99306-1a(2)	2.5699	64	Tabular	9	7	34	1646	19.68	83,644
	99323-1c(2)	2.56	40	Tabular	3	5	19	1890	14.55	129,875
	99303-2(2)	2.3346	39	Tabular	15	5	25	1386	16.73	82,812
	99318-1a(1)	2.2752	43	Tabular	7	8	21	2076	14.40	144,206
	99306-1a(1)	2.2295	24	Tabular	15	11	13	1760	11.80	149,222
	99302-2(1)	2.2087	38	Tabular	33	13	12	3004	11.31	265,721
	99323-1c(3)	1.635	24	Tabular	32	11	17	1387	13.25	104,678
	99305-3(2)	1.42	25	Tabular	64	9	96	255	31.34	8,126
	99305-3(1) 3ϕ	2.333	31	Tabular	25	5	62	435	26.81	16,220
	99305-3(1) 4ϕ	1.714	51	Tabular	50	6	117	374	37.03	10,090

from which images were taken. Each plagioclase crystal in an SEM image was measured to obtain the area (μm^2), perimeter (μm), crystal length (μm), width (μm) and aspect ratio (AR) using the image processing freeware, NIH Image (available from http://www.nih.gov). Analysis of several additional images was required for clasts with low crystal number density to make measurements of at least 50 crystals per sample (Hammer et al., 2000; Couch et al., 2003b). We then calculated plagioclase area fraction (Φ=total area of plagioclase crystals/total area of solid groundmass), average microlite area (μm^2), plagioclase area number densities, N_a (number of crystals/mm^2) and vesicle area per total sample area. Characteristic crystal size, s (μm) and volumetric number density N_v, were calculated by the following equations (following methods described in Hammer et al., 1999):

$$S = \left(\frac{\Phi}{N_a}\right)^{\frac{1}{2}} \quad (1)$$

$$N_v = \frac{N_a}{S} \quad (2)$$

Crystals that were cut off by the edge of the image were not included in individual crystal area measurements, but were included in measurements of total area fraction and number density.

3. Results

3.1. Natural sample characteristics

Plagioclase morphologies are mostly dominated by tabular crystals. Hopper, skeletal and spherulitic morphologies are rare, with a very limited number found among the smallest microlite population in Samples 1a, 6a and 6b (Table 1; Fig. 2). Characteristic crystal sizes vary widely from 3.4 μm to 37 μm and average microlite area ranges from 10 to nearly 200 μm^2. The maximum crystal AR per sample varies from 3 to 19, with >97% of observed crystals having AR <10, and seventeen of the twenty-three samples having maximum crystal AR ≤ 10. Because of the dominance of tabular low-AR crystals and lack of obvious crystal fabric, vol.% and area% are assumed to be equal (Russ, 1986; p. 105; e.g. Hammer et al., 1999; Cashman and Blundy, 2000).

Microlite crystal vol.% (as a percentage of total solid volume) ranges widely from 11 to 64 vol.% (±2%). Groundmass crystal number density, N_a, also varies widely: Samples 5a, 6a and 7a have nearly 20,000 crystals per mm^2, Samples 1b and 7b have approximately 10,000 crystals per mm^2, and the remaining natural samples have 300 to 7000 crystals per mm^2. N_a of the natural samples are generally consistent with the experimental samples

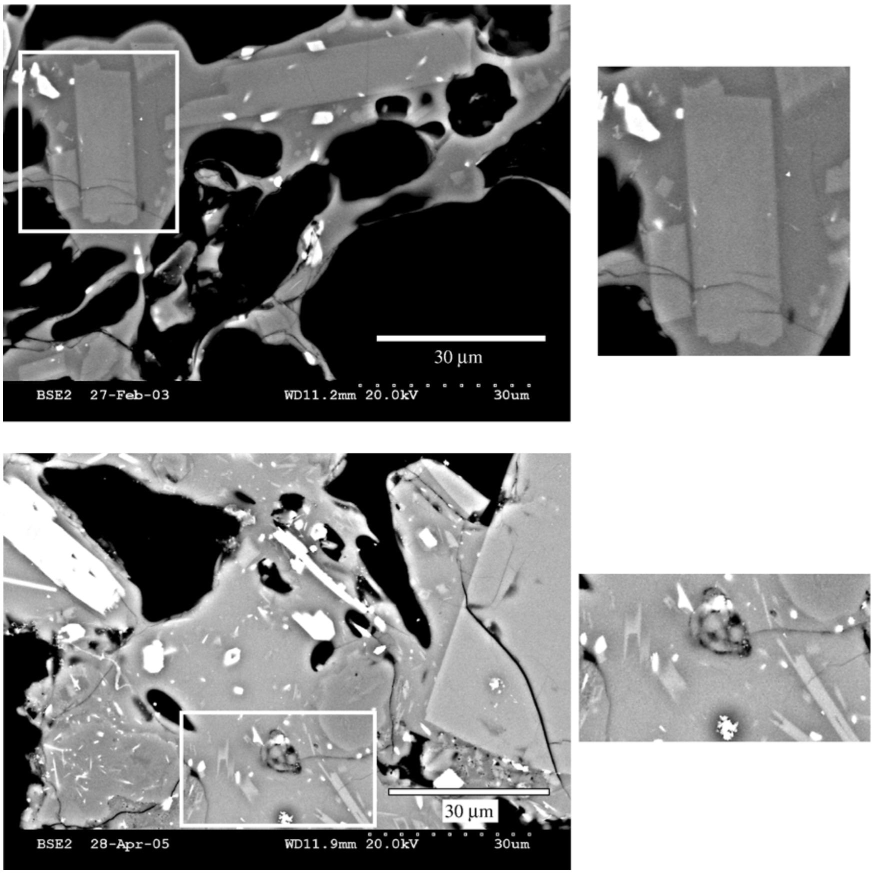

Fig. 2. Morphologies observed in this study. Most crystals exhibit tabular morphologies and have AR <10 (top), whereas hopper and spherulitic crystals are rare (bottom).

of Couch et al. (2003b), which have up to 13,000 crystals per mm^2 in one experiment, but typically range between 200 and 8000 crystals per mm^2.

Histograms of crystal area distributions show that more than 50% by number of the crystals in each sample are <20 µm^2. Nearly all natural sample plagioclase microlite area histograms follow the same trend, although the total number of microlites <20 µm^2 varies from 1500 to 12000. Fig. 3 shows the plagioclase area histogram for three natural samples, representing the full range of data, compared with experimental samples (Couch et al., 2003b). Samples 4b and 6b are more typical of natural samples, whereas Sample 1b has the largest number of <20 µm^2 crystals observed. Natural sample data is summarized in Table 1.

3.2. Determining style of decompression

We infer that our natural sample data are broadly consistent with MDE-style decompression to low final quench pressures (<50 MPa), with short residence times (<12 h), and large step size (>13.75 MPa), for the following reasons. First, an MDE decompression path is consistent with observations of the 1997 Vulcanian explosions (Druitt et al., 2002; Clarke et al., 2002a,b). Observations and models of the SHV Vulcanian explosions indicate repetitive magma ascent and shallow stagnation (Druitt et al., 2002; Clarke et al., 2002a,b) followed by evacuation of approximately 3×10^5 m^3 DRE of material from the conduit for a typical event (Druitt et al., 2002). Given a DRE density of 2600 kg m^{-3} (Sparks et al., 1998) and conduit diameter between 20 and 30 m (Voight et al., 1999), decompression of magma deeper in the conduit due to a single explosion was ~11–24 MPa. Magma remaining in the conduit then ascended in response to the unloading, and the process repeated on average every 9.5 h. Given magma chamber pressure of roughly 125–130 MPa (Rutherford et al., 1998; Barclay et al., 1998; Devine et al., 1998) and decompression magnitudes of 11–24 MPa for each explosion, a parcel of ascending magma experiences between five and twelve discrete decompressions during its path to the surface.

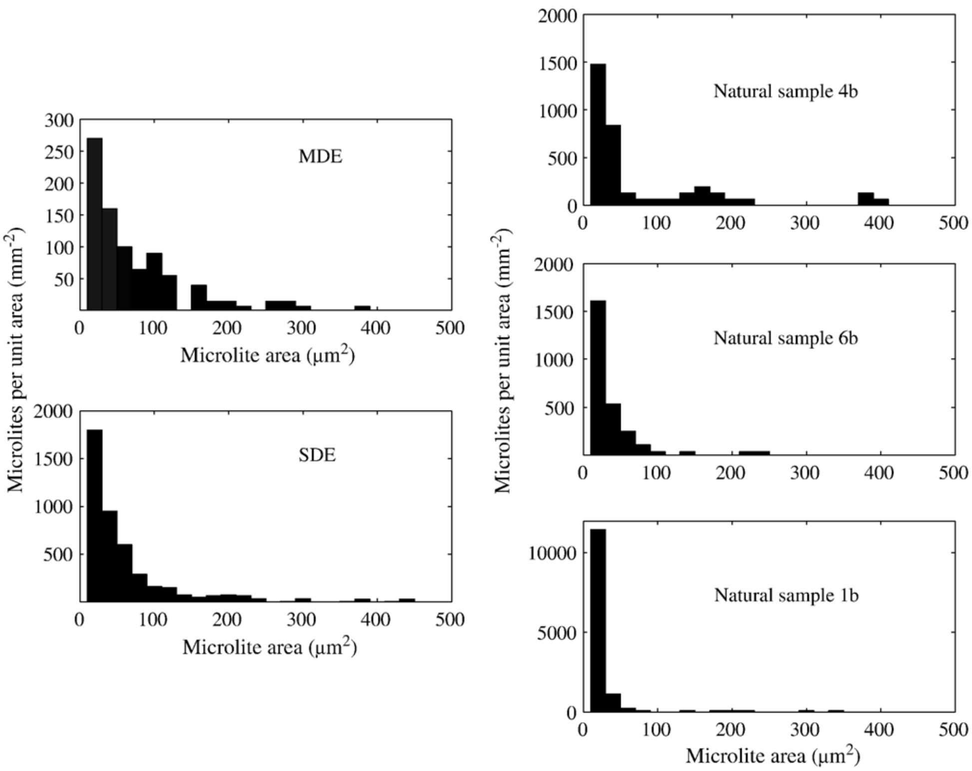

Fig. 3. Frequency distribution of microlite areas for experimental and natural samples. Trends differ slightly between MDE experiments (top left; ΔP = 13.75 MPa; T_r = 1 h; P_f = 50 MPa) and SDE experiments (bottom left; T_r = 24 h; P_f = 30 MPa). Samples 4b, 6b and 1b (right) represent the range found in natural samples. Note the different vertical scales.

Jaquet et al. (2006) estimated eight decompressions to explain time series statistics, corresponding to 17 MPa for each step and a total of 76 h between chamber and quench.

Second, crystal morphology strongly indicates MDE-style decompression. Crystal morphology is a better indicator of decompression rate and style than crystal abundances (Hammer and Rutherford, 2002). Crystal morphologies, largely tabular with AR <10, are consistent with MDE-style decompression or SDE-style decompression to quench pressures >125 MPa (Hammer and Rutherford, 2002; Couch et al., 2003b). However, because chamber pressure is estimated to be roughly 125–130 MPa (Rutherford et al., 1998; Barclay et al., 1998), the second possibility seems unlikely.

Third, microlite size distribution and total number of groundmass crystals suggest either SDE-style decompression with a long residence time (Fig. 3; P_f = 30 MPa, T_r = 24 h) or MDE decompression to P_f < 50 MPa. Experimental MDEs show that, with short residence times (<12 h), MDE crystal area histograms are converging toward patterns observed in the natural samples (Fig. 4; after Couch et al., 2003b); as ΔP increases and P_f decreases, the maximum peak in the histogram moves toward smaller crystals and becomes more distinct. Couch et al. (2003b) were not able to investigate small values of P_f because large increases in sample volume associated with decompressional degassing caused repeated rupture of sample containers (personal communication). Therefore MDE experiments go to P_f > 50 MPa whereas natural samples probably quenched at lower pressures, given that Druitt et al. (2002) estimated the depth of conduit evacuation to be <2 km.

Given these lines of evidence, we proceed by using experimental data from MDEs (8-h data for SHV), rather than SDEs, to estimate the quench pressure of each natural clast.

3.3. Estimating quench pressures

Fig. 5 shows experimental MDE data (groundmass vol.% feldspar vs. quench pressure) of both Couch et al. (2003b, see Table 1 — T_r = 8 h MDE data) and Hammer and Rutherford (2002, see Fig. 7d), along with a best-fit power law curve for each data set. By calculating CIPW

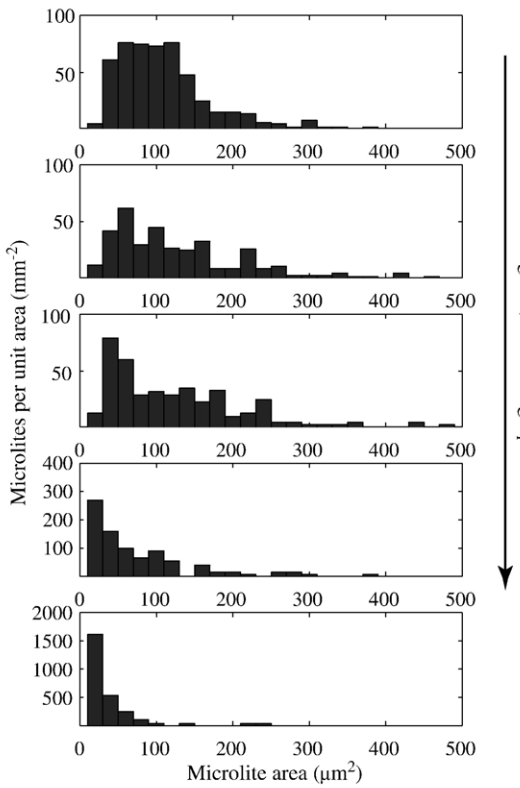

Fig. 4. Top four plots are microlite area frequency distributions from MDEs (T_r<12 h), with increasing ΔP and decreasing P_f from top to bottom (after Couch et al., 2003b). The bottom plot is Sample 6b. Note that the peak of the MDE histograms moves to the left and becomes more pronounced as ΔP increases and P_f decreases, and thus the MDE data appear to be converging toward the natural sample distribution.

norms at 1 bar (0.1 MPa), the maximum plagioclase crystallization possible is approximately 60 vol.% for the Pinatubo groundmass (Hammer and Rutherford, 2002) and 50–60 vol.% for the SHV groundmass (Fig. 5; grey square; Barclay et al., 1998; Devine et al., 1998), based on melt inclusion compositions. The change in curve fit for the Couch MDE data is imperceptible if 55 vol.%, rather than 60 vol.% at 0.1 MPa is used. Quench pressures of the natural samples were obtained by substituting groundmass feldspar vol.% into both power law relationships and averaging the values for each clast. It is this average which is reported throughout the remainder of the text as *quench pressure*. The Pinatubo data set was used as a constraint; the two systems have similar characteristics (at pressures >50 MPa and in maximum feldspar fraction), with the Hammer and Rutherford (2002) decompressions providing an additional data point at 5 MPa. Errors in quench pressure estimates are associated with ±2 vol.% uncertainty in plagioclase measurements for both natural and experimental samples.

We equate clast quench pressure with its pre-explosion depth in the conduit (or the depth from which the clast originated) by developing the following hypothesis with associated assumptions. Vulcanian explosions expose stagnated, high-pressure, gas-rich magma to atmospheric pressure (Turcotte et al., 1990; Alidibirov, 1994; Woods, 1995; Alidibirov and Dingwell, 1996). A rapidly moving fragmentation wave (30–70 m s^{-1}; Spieler et al., 2004b) moves down the conduit, quenching magma and ejecting a mixture of pyroclastic material and gas in its wake. The explosion ceases when the front reaches magma which does not satisfy conditions necessary for fragmentation (Papale, 1999; Zhang, 1999; Spieler et al., 2004a) and expulsion of pyroclastic material (Mason et al., 2006). The time scale of fragmentation and quench (~seconds) is much shorter than that of crystal nucleation and growth (minutes to hours; Couch et al., 2003a,b), thus the pre-

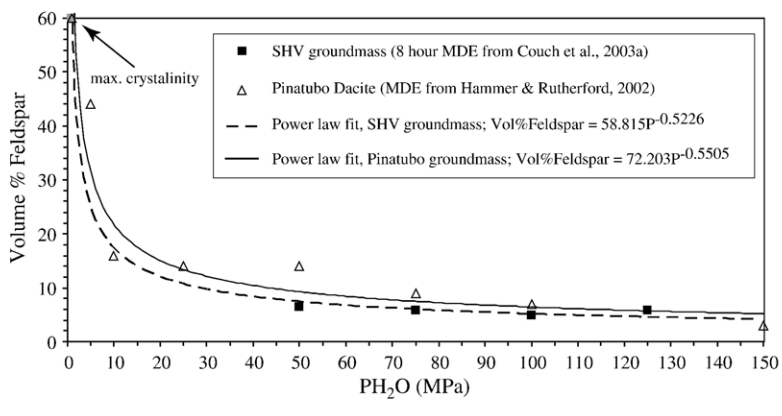

Fig. 5. Experimental MDE data of Hammer and Rutherford (2002; open triangles) and Couch et al. (2003b, 8-h MDE, closed squares); groundmass vol.% feldspar vs. quench pressure. Curves are power law fits of the experimental data; equations are in the legend. The grey square represents the maximum feldspar crystallinity possible for the SHV groundmass (50–60 vol.%), based on major element chemistry. The root mean square error of the average power law fit for pressure values <50 MPa is +/−2.2 MPa.

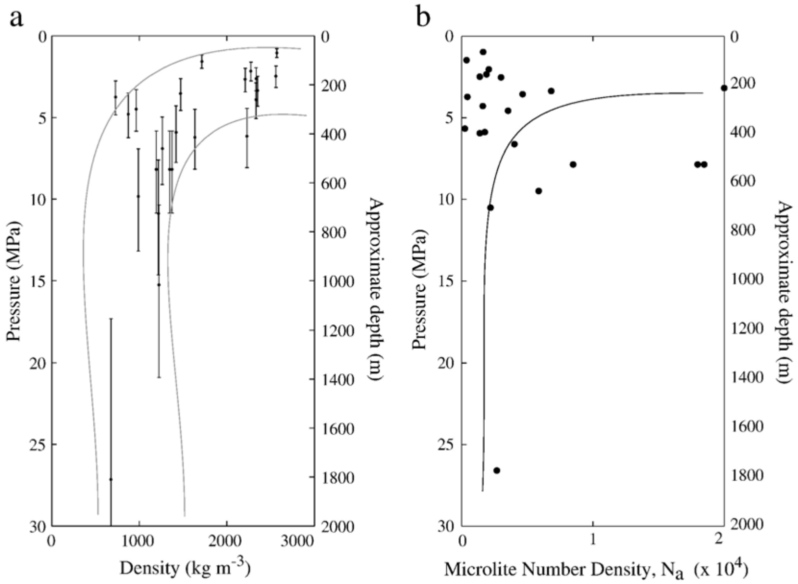

Fig. 6. (a) Estimated quench pressure vs. measured clast density; (b) estimated quench pressure vs. microlite number density, N_a. Corresponding approximate depth (right vertical axis) was estimated by assuming an average magma density of 1500 kg m^{-3}. Errors in quench pressure estimates are associated with ±2% uncertainty in measuring plagioclase vol.% of natural clasts and experimental samples. Errors in density measurements are represented by the diameter of the symbol. Errors in N_a are associated with uncertainty in vol.% measurements and are ±2%. Please note that the quench pressures presented here differ from those presented in Diller et al. (2006), although the general trends are the same. These values are final, while those of Diller et al. (2006) were preliminary.

explosion groundmass crystallinity is preserved in the ejected clasts and variations in groundmass crystallinity reflect the different depths at which the clasts resided prior to explosion. We also assume (first order) that bubble growth halted at explosion initiation. Formenti and Druitt (2003) found that syn-explosion bubble nucleation may occur, resulting in a uniformly distributed density change of <15%, which suggests that density trends with depth are approximately preserved. Pre-explosion conduit profiles of density and microlite number density (N_a) using quench pressure as a proxy for depth are shown in Fig. 6.

4. Discussion and interpretation

We now interpret these profiles (Fig. 6) within the context of magma ascent dynamics. Clast density gently decreases as quench depth shallows, until ~7 MPa (ranging from 3 to 11 MPa), at which point both density (Fig. 6a) and N_a (Fig. 6b) increase dramatically. We attribute the high density (1500–3000 kg m^{-3}) of the shallow samples to open-system degassing, which prevented further vesicle growth and reduced existing vesicularity (Eichelberger et al., 1986; Sparks, 1997; Melnik and Sparks, 1999, 2002; Takeuchi et al., 2005). The increase in crystal number density represents a transition from growth- to nucleation-dominated crystallization. Concurrent changes in clast density and crystal number density suggest a relationship between vesiculation, bubble connectivity and microlite nucleation. We interpret the relationship as follows: a burst of crystal nucleation occurs at the threshold pressure ~7 MPa, creating volatile supersaturation in the remaining melt, forcing further degassing, increasing melt viscosity, and initiating onset of brittle behavior and subsequent fractures in the system (Gonnermann and Manga, 2003; Tuffen et al., 2003). The sudden burst of nucleation also requires that bubbles occupy a smaller melt fraction, allowing high levels of bubble connectivity. Both fractures and high bubble connectivity promote permeable gas loss, resulting in vesicle collapse and a dense plug, potentially creating conditions favorable to Vulcanian explosions. Given average measured plug densities of ~2000 kg m^{-3} and pressures of 5–10 MPa at its base, the plug is approximately 250–700 m thick.

Alternatively, Kennedy et al. (2005) have suggested that density variations in Vulcanian eruptive products result from horizontal variations in the conduit, and that dense, near-wall parcels of magma are ejected via implosion during the later stages of an explosion. Although we agree that horizontal variations can exist in the conduit, the high groundmass crystallinity of many of our natural clasts clearly suggest residence time for hours rather than tens of seconds (the duration of an

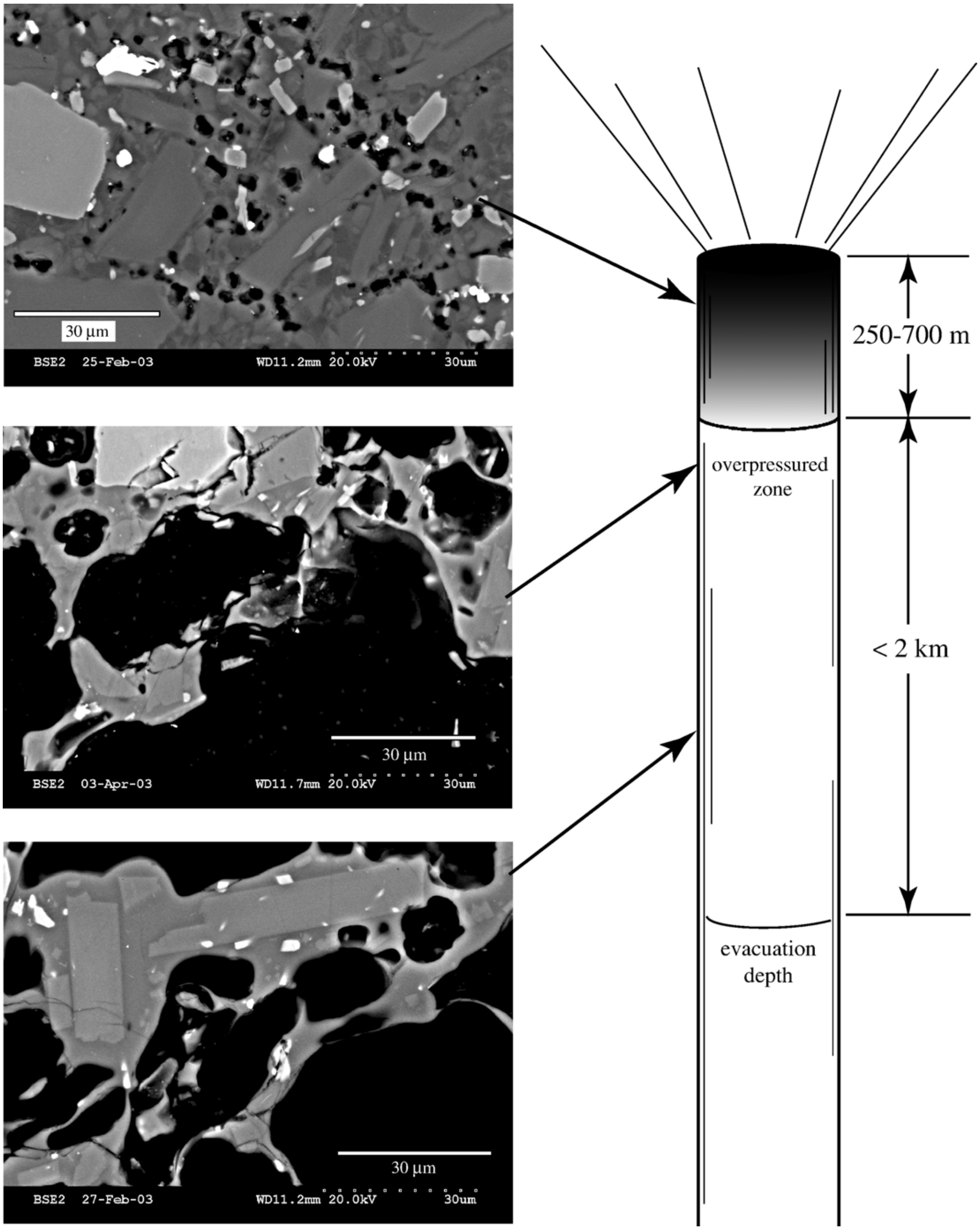

Fig. 7. Schematic representation of relative positions of sample types in the pre-explosion conduit. Dense plugging magma is evidenced by low-vesicularity clasts with a highly crystalline groundmass (top left), and occupies the top 250–700 m of the conduit. Magma immediately underlying the plug is highly vesicular (due to closed-system degassing) and has a moderately crystalline groundmass (middle left; overpressured zone). The 1997 Vulcanian explosions at Montserrat evacuated the conduit to depths of 2 km or less.

individual explosion) at low pressure, making our highly-crystalline, dense clasts more appropriately explained by shallow pre-explosion residence depths than by horizontal density variations.

Clasts originating from the base of the plug have the lowest densities in our sample set, indicating extensive closed-system degassing due to ascent to shallow levels, along with little to no gas escape from the system. This

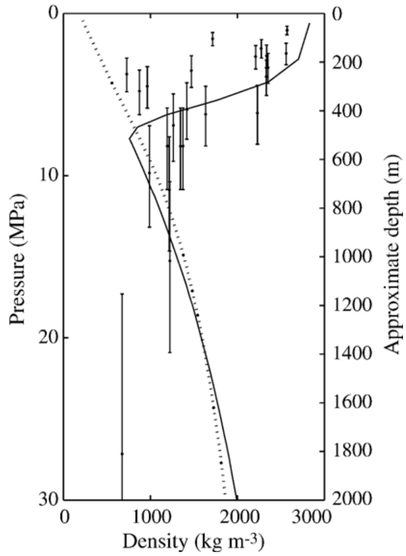

Fig. 8. Quench pressure vs. measured clast density (Fig. 6a), compared against 1D model results for an SHV magma ascending at 3.5 m^3 DRE s^{-1}; considering only vertical gas loss (dotted line) and considering both vertical gas loss and gas loss through conduit walls (solid line).

region of closed-system degassing may be the location of high overpressure which served as the source of observed surface deformation during the 1997 eruptive period at SHV. Deformation data and modelling place the center of overpressure between 400 and 900 m beneath the vent prior to explosion onset (Voight et al., 1998, 1999; Widiwijayanti et al., 2005), reasonably consistent with our estimates of plug thickness. The (gradual) transition from highly vesiculated conduit to the dense plug begins at bulk vesicularity of approximately 70% (density ≅ 700 kg m^{-3}), equivalent to slightly less than 90% vesicularity for the melt fraction, a value broadly consistent with both the relationship of Eichelberger et al. (1986), for which permeability increases by three orders of magnitude at approximately 60% vesicularity, and with the trend determined by recent experiments of Takeuchi et al. (2005), for which large increases in permeability (two orders of magnitude) occur between 45 and 80% vesicularity. Our data suggest that once the threshold is reached, permeability and open-system degassing persist until porosity is significantly reduced due to bubble collapse, and high bulk densities are reached (plug formation). Parcels of magma which have not yet reached the threshold porosity will have insignificant permeability (~10^{-17}–10^{-16} m^2; Takeuchi et al., 2005) and thus degas under closed-system conditions.

Natural samples with the lowest crystal area fractions had the deepest origins, with approximately 30 MPa equivalent to roughly 2 km depth (based on a conversion from pressure to depth via the average clast density of 1500 kg m^{-3}), consistent with evacuation depths of 1–2 km estimated for the same events by Druitt et al. (2002). Fig. 7 schematically shows the conduit profile.

5. Comparisons against models of 1D flow in a conduit

We now compare the data presented here against solutions independently generated by a one-dimensional axisymmetric model of magma ascent. Fig. 8 compares bulk density vs. pressure of two model calculations against the sample data. The numerical model is based on Melnik and Sparks (1999) with some variations relevant to this study (Appendix A; Diller et al., 2006). Here we consider only magma ascent between explosions in order to predict the stagnated, pre-explosion conduit profile. We first assume that magma ascends at a steady rate between explosions, during which time continuous permeable gas loss occurs, either in only the vertical direction or in both the vertical and horizontal directions simultaneously. We then assume that the pressure profile associated with steady ascent is preserved through the stagnation period. The model does not consider the highly unsteady transition between stagnation and Vulcanian explosion.

In this way, we calculate magma vesicularity (bulk density) and total pressure as functions of depth for a magma with 45% crystals suspended in a rhyolite melt (Murphy et al., 1998; Devine et al., 1998), steadily rising from 5 km depth (Barclay et al., 1998; Devine et al., 1998). The model accounts for exsolution of volatiles and gas escape due to system permeability, but does not directly include effects of crystal nucleation and growth. The numerical results shown are for flow rates of 3.5 m^3 DRE s^{-1}, within the range estimated for the 1997 period of Vulcanian explosions (Druitt et al., 2002). The first model run allows permeable gas loss only in the vertical direction (Fig. 8, dotted line; Eq. (A2), $Q_{gloss}=0$ and Eq. (A8)). This formulation does not predict the shallow dense cap supported by field observations (Druitt et al., 2002; Clarke et al., 2002a,b) and our petrologic data.

The addition of permeable conduit walls (1×10^{-13} m^2; Jaupart and Allegre, 1991) to the model (Eq. (A12)) predicts formation of the dense cap (Fig. 8, solid line). In this model case, gas loss is controlled by conduit overpressure and country rock permeability, such that gas loss through conduit walls goes to zero if conduit overpressure or country rock permeability go to zero. Conduit overpressure increases with magma viscosity (Sparks, 1997; Melnik and Sparks, 1999, 2002), which increases rapidly due to volatile exsolution and crystallization (Lejeune and Richet, 1995; Hess and Dingwell, 1996). Loss of volatiles through the conduit walls likely drives gasses to the surface via subvertical paths (Gonnermann and Manga, 2003), creating a region of degassing at the summit which is larger than the presumed conduit cross-sectional area. Although this model does not match all subtleties of the petrologic data, the general trends are consistent.

6. Conclusions

Comparing groundmass crystallinities of natural samples with controlled laboratory experiments provides significant insight into the pre-explosion conduit conditions of the 1997 SHV system. Groundmass plagioclase morphologies and size distributions suggest magma decompression from chamber to surface over several decompression steps of >13.75 MPa each, with inter-step residence times <12 h. The decompression pattern is consistent with conclusions based upon independent observations of the same events (Druitt et al., 2002) and statistical analysis of explosion time-series data (Jaquet et al., 2006). The maximum quench pressure revealed by our data is ~30 MPa (Fig. 6), corresponding to ~2 km depth, again consistent with field estimates of volume of magma erupted and depths of evacuation (Druitt et al., 2002). Density and crystal number density profiles suggest a critical pressure of ~7 MPa (range of 3 to 11 MPa), below which system permeability and crystal nucleation are significantly enhanced and potentially begin to control large-scale dynamics. At the same critical pressure magma vesicularity is ~70%, within the range of values corresponding to large increases in permeability according to measurements of natural samples (~60%; Eichelberger et al., 1986) and experimental products (45–80%; Takeuchi et al., 2005). According to 1D modeling results, permeable gas loss through porous media in the vertical direction alone cannot create a confining plug for 1997 SHV period of Vulcanian explosions, however, gas loss through permeable conduit walls can produce a conduit profile consistent with petrologic data.

Acknowledgements

We would like to thank John Wade, Stuart Kearns and Victoria Buckley of the University of Bristol Earth Sciences Department for assisting sample preparation and SEM image acquisition. Sample collection was made possible by the Montserrat Volcano Observatory and by a variety of field partners especially Rob Watts and Tappy Squires. We gratefully acknowledge the use of facilities within the Center for Solid State Science at Arizona State University. Financial support was provided by the Royal Society of London and the National Science Foundation (EAR-0310329). Comments by Mac Rutherford and one anonymous reviewer greatly improved the manuscript. Discussions with Julia Hammer, Susan Couch and Laura Wasylenki proved quite enlightening.

Appendix A. 1D model of magma ascent

The conservation of mass for both the magma (melt-crystal mixture) and gas phases are (following Melnik and Sparks, 1999):

$$\frac{\mathrm{d}}{\mathrm{d}z}(1-\alpha)\rho V = \frac{\mathrm{d}}{\mathrm{d}z}Q_{\mathrm{m}} = 0 \tag{A1}$$

$$\frac{\mathrm{d}}{\mathrm{d}z}\rho_{\mathrm{g}}\alpha V_{\mathrm{g}} + \frac{\mathrm{d}}{\mathrm{d}z}\rho_{x_{\mathrm{d}}}V = \frac{\mathrm{d}}{\mathrm{d}z}Q_{\mathrm{g}} = Q_{\mathrm{g_{loss}}} \tag{A2}$$

$$\rho = (\rho_{\mathrm{m}}(1-\beta)(1-x_{\mathrm{d}}) + \rho_{\mathrm{c}}\beta) \tag{A3}$$

$$\rho_{x_{\mathrm{d}}} = \rho_{\mathrm{l}}(1-\alpha)(1-\beta)x_{\mathrm{d}} \tag{A4}$$

where α is the gas volume fraction, β is the crystal volume fraction, x_{d} is the mass concentration of dissolved gas, ρ, ρ_{m}, ρ_{c}, ρ_{g}, and $\rho_{x_{\mathrm{d}}}$ are the densities of the magma, melt, crystals, gas and dissolved gas, respectively, z is depth in the conduit, V and V_{g} are the velocities of the magma and gas, respectively, and Q_{m} and Q_{g} are the discharge rates of magma and gas, respectively, per unit area. The mass concentration of water dissolved in the melt, x_{d}, was taken as 4.3+/−0.5 wt.% in the chamber (Devine et al., 1998; Barclay et al., 1998). Density of the melt was taken as 2300 kg m^{-3}, and the density of the crystals was taken as 2700 kg m^{-3} (Melnik and Sparks, 1999, 2002). Volumetric magma flux rate for the period of Vulcanian explosions was taken to be 3.5 m^3 s^{-1}, and the conduit diameter is 30 m. The density of the gas was calculated using the ideal gas law. We assume that the melt, crystals and gas are at 1133 K (860 °C), and the system is isothermal.

The equation for conservation of momentum for the system takes the following form:

$$\frac{\mathrm{d}p}{\mathrm{d}z} = -\rho_{\mathrm{mix}}g - \frac{32\mu_{\mathrm{mix}}V}{D^2} \tag{A5}$$

where:

$$\rho_{\mathrm{mix}} = (1-\alpha)(\rho_{\mathrm{m}}(1-\beta)(1-x_{\mathrm{d}}) + \rho_{\mathrm{c}}\beta) \tag{A6}$$

and p is pressure, ρ_{mix} is density of the melt–crystal–gas mixture, g is acceleration due to gravity, μ_{mix} is the viscosity of the melt–crystal–gas mixture, and D is the conduit diameter. Darcy's Law allows the melt and gas phases to move at different velocities, provided permeability is sufficient. Gas velocity is related to magma velocity via permeability, k, gas viscosity, μ_g, and vertical pressure gradient, dp/dz, as follows:

$$V_g - V = \frac{k(k_0, \alpha)}{\mu_g} \frac{dp}{dz} \tag{A7}$$

Permeability, $k(\alpha)$, is a function of gas volume fraction, as follows from Klug and Cashman (1996):

$$\log\left(\frac{k(\alpha)}{k_0}\right) = -10.2(100\alpha)^{\frac{0.014}{\alpha}} \tag{A8}$$

where k_0 is the reference permeability coefficient.

The viscosity of the melt phase is a function of the mass fraction of water dissolved in the melt, as determined experimentally by Hess and Dingwell (1996), as follows:

$$\log\mu_m = \frac{[-3.545 + 0.833\ln(x_d)] + [9601 - 2368\ln(x_d)]}{T - [195.7 + 32.25\ln(x_d)]} \tag{A9}$$

where μ_m is the melt viscosity in Pa s and T is the temperature in Kelvin. The viscosity of the mixture is described by the following equation, (Melnik and Sparks, 1999):

$$\mu_{mix} = \theta(\beta)\mu_m(x_d) \tag{A10}$$

where $\theta(\beta)$ is a function that represents the influence of crystals on the mixture viscosity as follows:

$$\log\left[\frac{\theta(\beta)}{\theta_0}\right] = \arctan[\omega(\beta - \beta^*)] + \frac{\pi}{2} \tag{A11}$$

where ω, β^*, and θ_0 are viscosity constants determined by viscosity and crystal volume fraction measurements on SHV dome rock (Melnik and Sparks, 1999). Gas loss through conduit walls was incorporated in the following way:

$$Q_{g_{loss}} = \frac{2\rho_g \alpha k_{cr}(p - p_{lith})}{\mu_g (D/2)^2} \tag{A12}$$

where Q_{gloss} is the rate of gas lost laterally, k_{cr} is the permeability of the surrounding country rock, and p and p_{lith} are magma and lithostatic pressure at a given depth. The total mass of gas lost laterally is simply accounted for by a deficit in the conservation of mass equation for the gas phase (Eq. (A2)). Gas loss is permitted through conduit walls only where two criteria are met: conduit overpressure with respect to lithostatic is greater than zero and the wallrock surrounding the conduit is permeable.

References

Alidibirov, M.A., 1994. A model for viscous magma fragmentation during volcanic blasts. Bull. Volcanol. 56 (6–7), 459–465.

Alidibirov, M.A, Dingwell, D.M., 1996. An experimental facility for the investigation of magma fragmentation by rapid decompression. Bull. Volcanol. 58 (5), 411–416.

Barclay, J., Rutherford, M.J., Carroll, M.R., Murphy, M.D., Devine, J.D., Gardner, J., Sparks, R.S.J., 1998. Experimental phase equilibria constraints on pre-eruptive storage conditions of the Soufrière Hills magma. Geophys. Res. Lett. 25 (18), 3437–3440.

Barmin, A., Melnik, O., Sparks, R.S.J., 2002. Periodic behavior in lava dome eruptions. Earth Planet. Sci. Lett. 199, 173–184.

Burnham, C.W., 1979. The importance of volatile constituents. In: Yoder, H.S. (Ed.), The Evolution of the Igneous Rocks: Fiftieth Anniversary Perspectives. Princeton University Press, pp. 439–482.

Cashman, K.V., 1992. Groundmass crystallization of Mount St. Helens dacite, 1980–1986: a tool for interpreting shallow magmatic processes. Contrib. Mineral. Petrol. 109, 431–449.

Cashman, K.V., Blundy, J., 2000. Degassing and crystallization of ascending andesite and dacite. Philos. Trans. R. Soc. Lond. 358 (1770), 1487–1513.

Cashman, K.V., McConnell, S.M., 2005. Multiple levels of magma storage during the 1980 summer eruptions of Mount St. Helens, WA. Bull. Volcanol. 68, 57–75.

Clarke, A.B., Voight, B., Neri, A., Macedonio, G., 2002a. Transient dynamics of vulcanian explosions and column collapse. Nature 415 (6874), 897–901.

Clarke, A.B., Neri, A., Voight, B., Macedonio, G., Druitt, T.H., 2002b. Computational modeling of the transient dynamics of the August 1997 vulcanian explosions at Soufrière Hills Volcano, Montserrat; influence of initial conduit conditions on near-vent pyroclastic dispersal. In: Druitt, T.H., Kokelaar, B.P. (Eds.), The eruption of Soufrière Hills Volcano, Montserrat, from 1995 to 1999. Geological Society of London Memoir, vol. 21, pp. 319–348.

Couch, S., Harford, C.L., Sparks, R.S.J., Carroll, M.R., 2003a. Experimental constraints on the conditions of formation of highly calcic plagioclase microlites at the Soufrière Hills Volcano, Montserrat. J. Petrol. 44 (8), 1455–1475.

Couch, S., Sparks, R.S.J., Carroll, M.R., 2003b. The kinetics of degassing-induced crystallization at Soufrière Hills Volcano, Montserrat. J. Petrol. 44 (8), 1477–1502.

Devine, J.D., Murphy, M.D., Rutherford, M.J., Barclay, J., Sparks, R.S.J., Carroll, M.R., Young, S.R., Gardner, J.E., 1998. Petrologic evidence for pre-eruptive pressure temperature conditions, and recent reheating, of andesitic magma erupting at the Soufrière Hills Volcano, Montserrat, W.I. Geophys. Res. Lett. 25 (19), 3669–3672.

Diller, K.D., Clarke, A.B., Voight, B., Neri, A., 2006. Mechanisms for Conduit Plug Formation: implications for Vulcanian explosions. Geophys. Res. Lett. 33, L20302. doi:10.1029/2006GL027391.

Druitt, T.H., Young, S.R., Baptie, B.J., Bonadonna, C., Calder, E.S., Clarke, A.B., Cole, P.D., Harford, C.L., Herd, R.A., Lockett, R., Ryan, G., Voight, B., 2002. Episodes of cyclic vulcanian explosive activity with fountain collapse at Soufrière Hills Volcano, Montserrat. In: Druitt, T.H., Kokelaar, B.P. (Eds.), The eruption of Soufrière Hills Volcano, Montserrat, from 1995 to 1999. Geological Society of London Memoir, vol. 21, pp. 281–306.

Eichelberger, J.C., Carrigan, C.R., Westrich, H.R., Price, R.H., 1986. Non-explosive silicic volcanism. Nature 323, 598–602.

Formenti, Y., Druitt, T.H., 2003. Vesicle connectivity in pyroclasts and implications for the fluidization of fountain-collapse pyroclastic flows, Montserrat (West Indies). Earth Planet. Sci. Lett. 214, 561–574.

Geschwind, C.H., Rutherford, M.J., 1995. Crystallization of microlites during magma ascent: the fluid mechanics of 1980–1986 eruptions at Mount St. Helens. Bull. Volcanol. 57, 356–370.

Gonnermann, H.M., Manga, M., 2003. Explosive volcanism may not be an inevitable consequence of magma fragmentation. Nature 426, 432–435.

Hammer, J.E., Rutherford, M.J., 2002. An experimental study of the kinetics of decompression-induced crystallization in silicic melt. J. Geophys. Res. 107, 148–227.

Hammer, J.E., Cashman, K.V., Voight, B., 2000. Magmatic processes revealed by textural and compositional trends in Merapi dome lavas. J. Volcanol. Geotherm. Res. 100, 165–192.

Hammer, J.E., Cashman, K.V., Hoblitt, R.P., Newman, S., 1999. Degassing and microlite crystallization during pre-climactic events of the 1991 eruption of Mt. Pinatubo, Philippines. Bull. Volcanol. 60, 355–380.

Hess, K.-U., Dingwell, D.B., 1996. Viscosities of hydrous leucogranitic melts: a non-Arrhenian model. Am. Mineral. 81, 94–108.

Hoblitt, R.P., Harmon, R.S., 1993. Bimodal density distribution of cryptodome dacite from the 1980 eruption of Mount St. Helens, Washington. Bull. Volcanol. 55 (6), 421–437.

Jaquet, O., Sparks, R.S.J., Carniel, R., 2006. Magma memory recorded by statistics of volcanic explosions at the Soufrière Hills Volcano, Montserrat. In: Mader, H.M., Coles, S., Connor, C. (Eds.), Statistics in Volcanology. Special Publications of IAVCEI, vol. 1, pp. 175–184.

Jaupart, C., 1998. Gas loss from magmas through conduit walls during eruption. The Physics of Explosive Volcanic Eruptions. Spec. Publ., vol. 145. Geol. Soc. London, pp. 75–92.

Jaupart, C., Allegre, C.J., 1991. Gas content, eruption rate and instabilities of eruption regime in silicic volcanoes. Earth Planet. Sci. Lett. 102, 413–429.

Kennedy, B., Spieler, O., Scheu, B., Kueppers, U., Taddeucci, J., Dingwell, D.B., 2005. Implosion during Vulcanian eruptions. Geology (Boulder) 33 (7), 581–584.

Klug, C., Cashman, K.V., 1996. Permeability development in vesiculating magmas: implications for fragmentation. Bull. Volcanol. 58, 87–100.

Lejeune, A.-M., Richet, P., 1995. Rheology of crystal-bearing silicate melts; an experimental study at high viscosities. J. Geophys. Res. 100 (3), 4215–4229.

Mason, R.M., Starostin, A.B., Melnik, O.E., Sparks, R.S.J., 2006. From Vulcanian explosions to sustained explosive eruptions: the role of diffusive mass transfer in conduit flow dynamics. J. Volcanol. Geotherm. Res. 153, 148–165.

Massol, H., Jaupart, C., 1999. The generation of gas overpressure in volcanic eruptions. Earth Planet. Sci. Lett. 166 (1–2), 57–70.

Mastin, L.G., 2005. The controlling effect of viscous dissipation on magma flow in silicic conduits. J. Volcanol. Geotherm. Res. 143, 17–28.

Melnik, O., Sparks, R.S.J., 1999. Nonlinear dynamics of lava dome extrusion. Nature 402, 37–41.

Melnik, O., Sparks, R.S.J., 2002. Dynamics of magma ascent and lava extrusion at Soufrière Hills Volcano, Montserrat. In: Druitt, T.H., Kokelaar, B.P. (Eds.), The eruption of Soufrière Hills Volcano, Montserrat, from 1995 to 1999. Geological Society of London Memoir, 21, pp. 153–170.

Melnik, O., Sparks, R.S.J., 2005. Dynamics of magma flow inside volcanic conduits with bubble overpressure buildup and gas loss through permeable magma. J. Volcanol. Geotherm. Res. 143 (1–3), 53–68.

Moore, G., Carmichael, I., 1998. The hydrous phase equilibria (to 3 kbar) of an andesite and basaltic andesite from western Mexico; constraints on water content and conditions of phenocryst growth. Contrib. Mineral. Petrol. 130 (3–4), 304–319.

Murphy, M.D., Sparks, R.S.J., Barclay, J., Carroll, M.R., Lejeune, A.M., Brewer, T.S., Macdonald, R., Black, S., Young, S., 1998. The role of magma mixing in triggering the current eruption at the Soufrière Hills volcano, Montserrat, West Indies. Geophys. Res. Lett. 25, 3433–3436.

Papale, P., 1999. Numerical simulations of magma ascent along volcanic conduits. Phys. Chem. Earth, Part A Solid Earth Geod. 24 (11–12), 957–961.

Russ, J.C., 1986. Practical Stereology. Plenum Press, New York. 194 pp.

Rutherford, M.J., Devine, J.D., Barclay, J., 1998. Changing magma conditions and ascent rates during the Soufriere Hills eruption on Montserrat. GSA Today 8 (3), 1–7.

Sisson, T.W., Grove, T.L., 1993. Experimental investigations of the role of H_2O in calc-alkaline differentiation and subduction zone magmatism. Contrib. Mineral. Petrol. 113 (2), 143–166.

Sparks, R.S.J., 1997. Causes and consequences of pressurisation in lava dome eruptions. Earth Planet. Sci. Lett. 150, 177–189.

Sparks, R.S.J., Young, S.R., Barclay, J., Calder, E.S., Cole, P., Darroux, B., Davies, M.A., Druitt, T.H., Harford, C., Herd, R., James, M., Lejeune, A.M., Loughlin, S., Norton, G., Skerrit, G., Stasiuk, M.V., Stevens, N.S., Toothill, J., Wadge, G., Watts, R., 1998. Magma production and growth of the lava dome of the Soufriere Hills Volcano, Montserrat, West Indies: November 1995 to December 1997. Geophys. Res. Lett. 25, 3421–3424.

Spieler, O., Dingwell, D.B., Alidibirov, M., 2004a. Magma fragmentation speed: an experimental determination. J. Volcanol. Geotherm. Res. 129, 109–123.

Spieler, O., Kennedy, B., Kueppers, U., Dingwell, D.B., Scheu, B., Taddeucci, J., 2004b. The fragmentation threshold of pyroclastic rocks. Earth Planet. Sci. Lett. 226 (1–2), 139–148.

Swanson, S.E., Naney, M.T., Westrich, H.R., Eichelberger, J.C., 1989. Crystallization history of Obsidian Dome, Inyo Domes, California. Bull. Volcanol. 51, 161–176.

Takeuchi, S., Nakashima, S., Akihiko, T., Shinohara, H., 2005. Experimental constraints on the low gas permeability of vesicular magma during decompression. Geophys. Res. Lett. 32, L10312. doi:10.1029/2005GL022491.

Taylor, B.E., Eichelberger, J.C., Westrich, H.R., 1983. Hydrogen isotope evidence of rhyolitic magma degassing during shallow intrusion and eruption. Nature 306, 541–545.

Tuffen, H., Dingwell, D.B., Pinkerton, H., 2003. Repeated fracture and healing of silicic magma generate flow banding and earthquakes? Geology (Boulder) 31 (12), 1089–1092.

Turcotte, D.L., Ockendon, H., Ockendon, J.R., Cowley, S.J., 1990. A mathematical model for vulcanian eruptions. Geophys. J. Int. 103, 211–217.

Voight, B., Sparks, R.S.J., Miller, A.D., Stewart, R.C., Hoblitt, R.P., Clarke, A.B., Ewart, J., MVO Staff, 1999. Magma flow instability and cyclic activity at Soufrière Hills Volcano, Montserrat. Science 283 (5405), 1138–1142.

Voight, B., Hoblitt, R.P., Clarke, A.B., Lockhart, A.B., Miller, A.D., Lynch, L., MacMahon, J., 1998. Remarkable cyclic ground deformation monitored in real time on Montserrat and its use in eruption forecasting. Geophys. Res. Lett. 25 (18), 3405–3408.

Widiwijayanti, C., Clarke, A.B., Elsworth, D., Voight, B., 2005. Geodetic constraints on the shallow magma system at Soufrière Hills Volcano, Montserrat. Geophys. Res. Lett. 32, L11309. doi:10.1029/2005GL022846.

Woods, A.W., 1995. A model of vulcanian explosions. Nucl. Eng. Des. 155, 345–357.

Woods, A.W., Koyaguchi, T., 1994. Transitions between explosive and effusive eruptions of silicic magmas. Nature 370, 641–644.

Young, S.R., Sparks, R.S.J., Aspinall, W.P., Lynch, L.L., Miller, A.D., Robertson, R.E.A., Shepherd, J.B., 1998. Overview of the eruption of Soufrière Hills volcano, Montserrat, 18 July 1995 to December 1997. Geophys. Res. Lett. 25 (18), 3389–3392.

Zhang, Y., 1999. A criterion for the fragmentation of bubbly magma based on brittle failure theory. Nature 402, 648–650.